

1  
2 **Observations of Suprathermal Electrons in Mercury's**  
3 **Magnetosphere during the Three MESSENGER Flybys**  
4

5 George C. Ho<sup>1\*</sup>, Richard D. Starr<sup>2</sup>, Robert E. Gold<sup>1</sup>, Stamatios M. Krimigis<sup>1,3</sup>, James A. Slavin<sup>4</sup>,  
6 Daniel N. Baker<sup>5</sup>, Brian J. Anderson<sup>1</sup>, Ralph L. McNutt, Jr.<sup>1</sup>, Larry R. Nittler<sup>6</sup>, Sean C. Solomon<sup>6</sup>  
7  
8  
9

10 <sup>1</sup>The Johns Hopkins University Applied Physics Laboratory, Laurel, MD 20723, USA

11 <sup>2</sup>Physics Department, The Catholic University of America, [Washington, DC 20064](#), USA

12 <sup>3</sup>Academy of Athens, Office of Space Research and Technology, Soranou Efesiou 4, Athens  
13 11527, Greece

14 <sup>4</sup>Heliophysics Science Division, NASA Goddard Space Flight Center, [Greenbelt, MD 20771](#),  
15 USA

16 <sup>5</sup>Laboratory for Atmospheric and Space Physics, [University of Colorado, Boulder, CO 80303](#),  
17 USA

18 <sup>6</sup>Department of Terrestrial Magnetism, Carnegie Institution of Washington, Washington, DC  
19 20015, USA  
20

21 **DRAFT**  
22

23 Received \_\_\_\_\_; accepted \_\_\_\_\_  
24

25 \*Corresponding author contact information: George.Ho@jhuapl.edu; phone 1-240-228-7083; fax: 1-240-228-0386  
26

27 November 23, 2010  
28  
29

30 **Abstract**

31 In 2008 the MESSENGER spacecraft made the first direct observation of Mercury's  
32 magnetosphere in the more than 30 years since the Mariner 10 encounters. During  
33 MESSENGER's first flyby on 14 January 2008, the interplanetary magnetic field (IMF) was  
34 northward immediately prior to and following MESSENGER's equatorial passage through this  
35 small magnetosphere. The Energetic Particle Spectrometer (EPS), one of two sensors on the  
36 Energetic Particle and Plasma Spectrometer instrument that responds to electrons from ~35 keV  
37 to 1 MeV and ions from ~35 keV to 2.75 MeV, saw no increases in particle intensity above  
38 instrumental background (~5 particles/cm<sup>2</sup>-sr-s-keV at 45 keV) at any time during the probe's  
39 magnetospheric passage. During MESSENGER's second flyby on 6 October 2008, there was a  
40 steady southward IMF, and intense reconnection was observed between the planet's magnetic  
41 field and the IMF. However, once again EPS did not observe bursts of energetic particles similar  
42 to those reported by Mariner 10 from its March 1974 encounter. On 29 September 2009,  
43 MESSENGER flew by Mercury for the third and final time before orbit insertion in March 2011.  
44 Although a spacecraft safe-hold event stopped science measurements prior to the outbound  
45 portion of the flyby, all instruments recorded full observations until a few minutes before closest  
46 approach. In particular, the MESSENGER Magnetometer documented several substorm-like  
47 signatures of extreme loading of Mercury's magnetotail, but again EPS measured no energetic  
48 ions or electrons above instrument background during the inbound portion of the flyby.  
49 MESSENGER's X-Ray Spectrometer (XRS) nonetheless observed photons resulting from low-  
50 energy (~10 keV) electrons impinging on its detectors during each of the three flybys. We infer  
51 that suprathermal plasma electrons below the EPS energy threshold caused the bremsstrahlung  
52 seen by XRS. In this paper, we summarize the energetic particle observations made by EPS and

53 XRS during MESSENGER's three Mercury flybys, and we revisit the observations reported by  
54 Mariner 10 in the context of these new results.

55

56

57 Keywords: Mercury, Magnetosphere, Energetic particles, MESSENGER

58 **1. Introduction**

59 The Mariner 10 (M10) spacecraft flew by Mercury three times in 1974 and 1975 and made  
60 measurements inside Mercury's magnetosphere during its first and third (M10-I and M10-III,  
61 respectively) encounters. The M10 in-situ measurements not only showed that Mercury  
62 possesses an intrinsic magnetic field (Ness et al., 1974), they also revealed substorm-like  
63 energetic particle bursts (Simpson et al., 1974) within the magnetosphere. However, ambiguities  
64 in the interpretation of the M10 energetic particle detector data were pointed out by Armstrong et  
65 al. (1975, 1979). In particular, there are difficulties extracting sufficient energy to accelerate  
66 highly repetitive bursts of high-energy (>600 keV) electrons in Mercury's small magnetosphere  
67 (Russell et al., 1988). Alternative scenarios to explain the source and acceleration of these  
68 reportedly high-energy electrons were put forward by Eraker and Simpson (1979), Baker (1986),  
69 and Luhmann et al. (1998). A summary of M10 energetic particle observations and their  
70 interpretation has been given by Wurz and Blomberg (2001). From the limited set of in-situ  
71 data obtained by M10, it is safe to conclude that the identity of the particles measured remains  
72 uncertain.

73 Given the controversy over the interpretation of the M10 particle observations, new  
74 measurements are needed to gain insight into the particle population in Mercury's  
75 magnetosphere. NASA's MErcury Surface, Space ENvironment, GEochemistry, and Ranging  
76 (MESSENGER) spacecraft flew by Mercury on 14 January 2008 (M1), 6 October 2008 (M2),  
77 and 29 September 2009 (M3) to perform gravity while en route to a scheduled insertion into orbit  
78 about the innermost planet in March 2011 (Solomon et al., 2007). During these three flybys, the  
79 spacecraft's particle and field instruments returned the first direct measurements of Mercury's  
80 magnetosphere in the 33 years since the last M10 encounter.

81 At the times of MESSENGER's three flybys, the component of the interplanetary magnetic  
82 field (IMF) normal to Mercury's orbital plane exhibited all three possible orientations: steadily  
83 northward (M1), steadily southward (M2), and varying between north and south (M3). As a  
84 result, Mercury's magnetosphere exhibited markedly different plasma and magnetic field  
85 signatures during the three encounters (Slavin et al., 2009a, 2009b, 2010). The Energetic  
86 Particle Spectrometer (EPS), one of two sensors that comprise the Energetic Plasma and Particle  
87 Spectrometer (EPPS) instrument (Andrews et al., 2007) on the MESSENGER spacecraft, did not  
88 detect any  $>35$  keV electron and ion fluxes above instrument background during any of the three  
89 flybys. This finding contrasts with what was originally reported from measurements made by the  
90 M10 particle instrument during M10-I. Nonetheless, measurements by MESSENGER's X-Ray  
91 Spectrometer (XRS) are here interpreted to be indicative of low-energy ( $\sim 10$  keV) electrons  
92 impinging on its detectors during the three flybys.

93 The purpose of this paper is to describe the response of the EPS sensor during all three flybys  
94 through the magnetosphere and correlate these with the observations reported by  
95 MESSENGER's Magnetometer instrument that delineated the magnetospheric topology. We  
96 then describe and model the XRS sensor responses and deduce the electron spectrum that  
97 resulted in the detection of X-ray photons. Finally, we revisit the observations reported by  
98 Mariner 10 in light of these new results.

99

## 100 **2. The MESSENGER Energetic Particle and X-ray Spectrometers**

101 The EPPS package on MESSENGER measures both the in-situ plasma composition and  
102 energetic particles (Andrews et al., 2007). EPS measures the energy, angular, and compositional  
103 distribution of the high-energy components of the in-situ electrons ( $> 35$  keV) and ions ( $> 5$

104 keV/nucleon), and the Fast Imaging Plasma Spectrometer (FIPS) measures the energy, angular  
105 distribution, and composition of the low-energy ion population.

106 The EPS is a time-of-flight (TOF) spectrometer with two main components: a TOF section  
107 with a 6-cm flight path and a solid-state detector (SSD) array. Particles enter the system through  
108 a collimator that delimits the look direction. They then transit a set of thin composite foils and  
109 strike the SSD array at the end of the TOF section. Secondary electrons generated by the  
110 particles (mostly ions) as they transit the foils are focused and detected by a set of microchannel  
111 plates (MCPs). Hence, ion composition can be measured for H to Fe from ~35 keV to ~3 MeV  
112 with the TOF section. Unfortunately, after launch the MCP voltage could not be raised to its  
113 nominal operating value in order to measure the TOF values. Hence, ion composition data from  
114 EPS have never been realized.

115 Nonetheless, the EPS SSD array at the back of the TOF section is operating nominally, so  
116 total ion and electron counts can be measured by EPS. The EPS SSD array uses 500- $\mu\text{m}$ -thick  
117 ion-implanted silicon solid-state detectors to measure the total energy of a particle; a thin layer  
118 (1- $\mu\text{m}$ ) of aluminum on the top of the detector discriminates the low-energy ion from the  
119 electrons. An electron that has energy higher than the threshold (~35 keV), however, will deposit  
120 energy in both the ion and electron SSDs. There are six parallel electronics signal-processing  
121 chains dedicated to the ion detectors and six parallel electronics signal-processing chains  
122 dedicated to the electron detectors. Hardware counters from separate discriminators provide a  
123 measure of whether particle pile-up is occurring (Andrews et al., 2007), a problem identified  
124 with the M10 detectors in the presumed high-flux environment during that flyby (Armstrong et  
125 al., 1975). Indeed, data from MESSENGER's Earth flyby showed that by using both the fast and

126 shaped discriminator measurements the EPS was not subject to saturation even in the most  
127 intense regions of the inner radiation belt.

128 The X-ray Spectrometer (XRS) on MESSENGER is designed to measure the soft X-ray  
129 fluorescence (1-10 keV) from Mercury induced by solar X-ray illumination of its surface. The  
130 XRS instrument consists of two major units, a silicon-PIN solar monitor mounted on the  
131 spacecraft sunshade that measures the solar X-ray flux and three gas proportional counters  
132 (GPCs) that are mounted on the spacecraft nadir-pointing deck and designed to detect  
133 fluorescence from Mercury's surface (Schlemm et al., 2007). A Be-Cu collimator restricts the  
134 field-of-view (FOV) of the GPC unit to 12°. The entrance windows of two of the GPCs are  
135 covered with thin foils of Mg (4.5- $\mu\text{m}$ ) and Al (6.3- $\mu\text{m}$ ), respectively, to allow separation of the  
136 low-energy fluorescence lines of Mg, Al, and Si. As will be discussed below, during the three  
137 Mercury flybys, the XRS recorded signals, including fluorescence of the Mg and Al filters,  
138 which were almost certainly caused by interactions with electrons from the magnetosphere.

139

### 140 **3. Observations**

#### 141 *3.1. Extremely quiet solar conditions*

142 Solar activity has been extremely low since late 2007, including the times of three Mercury  
143 flybys. The observed sunspot numbers in 2008 were at the lowest level since the beginning of  
144 space age (see <http://www.swpc.noaa.gov/>). Particle instruments on spacecraft throughout the  
145 heliosphere have reported minimal solar energetic particle intensities, whereas the galactic  
146 cosmic ray intensities are at their highest level in 50 years  
147 ([http://science.nasa.gov/headlines/y2009/29sep\\_cosmicrays.htm](http://science.nasa.gov/headlines/y2009/29sep_cosmicrays.htm)). Hence, even though EPPS has

148 been on and taking data almost continuously since June 2007, no major solar energetic particle  
149 (SEP) events have been detected above the EPS background rate ( $\sim 0.1 \text{ s}^{-1}$ ), with one exception.

150 Two weeks before M1, on 31 December 2007, MESSENGER observed a solar flare that was  
151 seen at the same time in soft X-rays by the Geostationary Operational Environmental Satellite  
152 (GOES) system and classified on the basis of those observations to be at least C8. However, the  
153 event occurred beyond the eastern limb of the Sun from the point of view of GOES, and analysis  
154 of X-rays detected from this event by the MESSENGER XRS indicates a flare magnitude of M2  
155 (Feldman et al., 2010). Profiles of intensity versus time for selected electron energy channels  
156 from EPS during this event are shown in Fig. 1. From timing and modeling, we conclude that  
157 the event was composed primarily of electrons and was also associated with solar neutrons as  
158 reported by the Neutron Spectrometer on MESSENGER (Feldman et al., 2010). Since the 31  
159 December 2007 event, there have not been any other such events detected by MESSENGER,  
160 although several have been seen by the Advanced Composition Explorer (ACE) Electron,  
161 Proton, and Alpha Monitor (EPAM) at 1 AU. Typical intensities at ACE, however, were at least  
162 a factor of 10 lower than the equivalent EPS background of  $\sim 2 \times 10^3 \text{ (cm}^2 \text{ s sr MeV)}^{-1}$ .

163

### 164 *3.2. Modeling of solar wind conditions*

165 As part of the United States' space weather effort, the National Science Foundation (NSF) has  
166 established the Center for Integrated Space Weather Monitoring (CISM). The CISM program,  
167 together with the National Oceanic and Atmospheric Administration (NOAA) Space Weather  
168 Predictions Center (SWPC), produces space environment predictions for the inner heliosphere.  
169 Baker et al. (2009) presented CISM predictions for the Mercury space environment at the time of  
170 the first MESSENGER flyby. Relatively slow solar wind conditions (solar wind velocity  $V_{\text{sw}} \sim$

171 400 km/s) were modeled, and predicted solar wind density values ( $n \sim 60\text{-}70 \text{ cm}^{-3}$ ) were also  
172 moderate as shown by Baker et al. (2010).

173

### 174 *3.3.EPS observations*

175 An overview of the field and particle measurements during M1 is shown in Fig. 2. As  
176 detailed by Slavin et al. (2008) and Anderson et al. (2008), the generally northward IMF was  
177 unfavorable to substorm-like particle energization processes (see Baker et al., 1996). On the  
178 basis of magnetic field measurements from the MESSENGER Magnetometer (MAG) and  
179 plasma measurements from FIPS, there was little evidence for reconnection between the IMF  
180 and the planetary magnetic field during M1 (Slavin et al., 2009b).

181 Energy spectra of the energetic particles measured by the EPS detector (including both ions  
182 and electrons) before, during, and after the M1 magnetospheric passage are shown in Fig. 3a.  
183 There were no differences in the spectral shape among the three time periods. The geometric  
184 factor of each EPS SSD is small ( $10^{-3} \text{ cm}^2\text{-sr}$ ), with no noticeable foreground from the  
185 environment; the instrument measured only high-energy galactic cosmic rays ( $> 10 \text{ MeV}$ ). High-  
186 energy cosmic rays will penetrate the instrument outer skin and deposit a minimum-ionizing  
187 energy in the SSD detectors as a broad peak around  $\sim 150 \text{ keV}$ , as shown in Fig. 3.

188 During M2, MESSENGER's trajectory was very similar to that during M1, with the  
189 spacecraft remaining nearly in Mercury's equatorial plane, approaching the planet from the night  
190 side and exiting on the dayside dawn sector. Note that between M1 and M2, the EPS energy  
191 channels and background were changed (as seen in Figs. 2, 3 and 4), because a flight software  
192 change was uploaded to EPPS in August 2008 to enhance the sensor telemetry and improve the  
193 background. During M2, Mercury's magnetosphere was noticeably different from its condition

194 during M1. A steady southward IMF led to classic reconnection signatures; flux-transfer events  
195 (FTEs) were observed in the magnetosheath and a plasmoid and multiple traveling compression  
196 regions were observed in Mercury's magnetotail (Slavin et al., 2009b). EPS and MAG  
197 measurements during M2 are shown in Fig. 4, and the particle energy spectra measured by EPS  
198 are shown in Fig. 3b. Surprisingly, other than the drop in particle intensity at closest approach  
199 due to the shadowing effect of the planet on cosmic rays, there was no burst of energetic particles  
200 detected by EPS similar to that reported by the M10 particle instrument. From this null result,  
201 and with the lowest energy channel on EPS covering 36-57 keV, we estimate that the ~ 45-keV  
202 electron intensity in Mercury's magnetosphere was not more than 5 particles/cm<sup>2</sup>/s/sr/keV.

203 The third and final flyby of MESSENGER at Mercury occurred on 29 September 2009.  
204 Immediately prior to the encounter, the IMF displayed a strong field magnitude (~28 nT) and  
205 variable north-south orientation (Fig. 5). (No detection was possible during the outbound portion  
206 of the M3 trajectory because of the spacecraft safe-hold event.) Slavin et al. (2010) reported  
207 multiple episodes of loading and unloading of the planetary magnetotail once the spacecraft was  
208 inside Mercury's magnetosphere, in a pattern qualitatively similar to substorm-like signatures  
209 commonly observed at Earth. A key signature of tail unloading during terrestrial substorms is  
210 the acceleration of energetic particles, but once again no acceleration signatures were seen by  
211 EPS up to closest approach (Fig. 5).

212

### 213 *3.4.XRS observations*

214 During all three flybys, the XRS measured several count-rate spikes within minutes of closest  
215 approach, both before (M1, M2, and M3) and after (M2) closest approach. The timing of four of  
216 these events is indicated in Figures 2, 4, and 5. Those occurring before closest approach are here

217 termed called M1-E1, M2-E1, and M3-E1. The event that followed M2 closest approach is  
218 termed M2-E2. The signatures of these four count-rate spikes clearly identify their origin as  
219 energetic electrons (~10-30 keV) interacting with the XRS detector material. Electron-induced  
220 fluorescence and bremsstrahlung are evident in the XRS gas proportional counters as shown in  
221 Fig. 6 and described in more detail below (see also Adler and Trombka, 1977 and Starr et al.,  
222 2000). Other increases in the XRS count rates seen during the two flybys, especially during M1,  
223 do not show fluorescence of the filter materials, have a very different spectral shape, and are  
224 most likely the result of increased photon fluxes originating from outside the XRS GPC  
225 detectors. For example, the Crab Nebula was in the XRS FOV during one such XRS count rate  
226 increase ~30 hours prior to M1, and modeling confirms that supernova remnant was the source  
227 of the observed X-rays. The source of the photon event following the M1 closest approach is not  
228 yet certain, but the galactic center was within the XRS FOV at this time, making it likely that this  
229 event, too, was from an astrophysical source. Only the four clearly electron-induced events near  
230 flyby closest approaches will be discussed here.

231 The XRS response to charged-particle interactions has been modeled and verified by  
232 measurements with the XRS engineering unit using the Potential Drop Accelerator at the  
233 Radiation Effects Facility ([http://radhome.gsfc.nasa.gov/radhome/ref/GSFC\\_REF.html](http://radhome.gsfc.nasa.gov/radhome/ref/GSFC_REF.html)) of the  
234 NASA Goddard Space Flight Center. The XRS instrument response was modeled with the  
235 Monte Carlo N-Particle eXtended (MCNPX) code (Pelowitz, 2005). Spectra measured during  
236 the flybys are well modeled by kappa-function electron distributions impinging on the XRS Mg  
237 and Al filters, Be windows, and Be-Cu collimator (Christon, 1987). The peaks at low energy  
238 seen in the plots for the Mg- and Al-filtered detectors in Fig. 6 correspond to the K-alpha lines  
239 for those two materials, at 1.254 and 1.487 keV, respectively. The broad peak at higher energy

240 seen in all three detectors during the M2-E2 event is from the Cu K-alpha line at 8.048 keV,  
241 produced by electron interactions in the Be-Cu collimator. Modeled results are compared to the  
242 measured X-ray spectra during events M1-E1 and M2-E2 in Fig. 6. For event M1-E1, the  
243 electron incidence angle is modeled as  $0^\circ$ , while for the M2-E2 event the incidence angle is  
244 modeled as  $6^\circ$ . The electron incidence angle determines the relative intensity of the Cu line and  
245 was varied to obtain the best fit between model and data. Model parameters are listed in Table 1.  
246 The absolute electron fluxes derived from the models are shown in Fig. 7, and the model  
247 parameters are given in Table 1. These electron fluxes are generally consistent with those  
248 predicted by the empirical model of Mukai et al. (2004) at 0.31 AU. During the flybys the  
249 MESSENGER spacecraft was at about 0.3 AU. The solar wind density was  $\sim 60 \text{ cm}^{-3}$ ,  $\sim 60 \text{ cm}^{-3}$ ,  
250 and  $\sim 50 \text{ cm}^{-3}$  during M1, M2, and M3, respectively (Baker et al., 2010).

251 The electron flux fit to the XRS data is consistent with the EPS upper limit at 45 keV for the  
252 three fluorescence events detected prior to closest approach (M1-E1, M2-E1, and M3-E1).  
253 However, for the second of the two M2 events (M2-E2), which followed closest approach, Cu  
254  $K\alpha$  fluorescence at 8 keV from the Be-Cu collimator, clearly indicates the presence of a much  
255 higher flux of electrons at energies greater than 10 keV. A good match to the XRS spectra  
256 (right-hand panels of Fig. 6) requires that the inferred electron intensity at 45 keV be  $\sim 100$  times  
257 higher than the EPS upper limit at 45 keV as indicated in Fig. 7. The difference between the two  
258 results can be explained by the different FOVs for XRS and EPS.

259 The XRS is mounted on the bottom deck of the spacecraft and has a conical  $12^\circ$  FOV along  
260 the spacecraft +Z axis, whereas the EPS has a fan-shaped FOV that looks away from the  
261 spacecraft sunshade along the spacecraft +Y axis (Fig. 8a) (Schlemm et al., 2007; Andrews et al.,  
262 2007). Only for event M2-E1 was the magnetic field orientation favorable for the simultaneous

263 observation of electrons by both EPS and XRS, but the estimated electron intensity inferred from  
264 the XRS measurement is below the EPS sensitivity level. However, during M2-E2, the  
265 measured local magnetic field vector was perpendicular to the XRS normal, which is necessary  
266 for XRS detection but very unfavorable for EPS to measure the short-duration electron event  
267 detected by XRS (Fig. 8a). This geometry also implies that the electron pitch-angle distribution  
268 was narrowly peaked near  $90^\circ$ , consistent with the modeled incidence angle ( $6^\circ$ ).

269

#### 270 **4. Reconciliation of the M10 and MESSENGER results?**

271 During the first Mariner 10 flyby of Mercury, four high-energy ( $>300$  keV) particle events  
272 during the encounter and a high-energy ( $> 600$  keV) proton event were reported (Simpson et al.,  
273 1974). For three of the four events, the time-intensity profiles had very sudden onsets, and the  
274 peak intensity levels were at least three orders of magnitude above interplanetary background  
275 levels (Simpson et al., 1974). However, no such high-energy particles were detected by  
276 MESSENGER during any of the three flybys.

277 There could be several factors that contribute to the differences in observations between M10  
278 and MESSENGER. The energetic particle instrument on M10 was designed to measure high-  
279 energy electrons ( $>170$  keV) and ions ( $>600$  keV) (Simpson et al., 1977; Wurz and Blomberg  
280 2001). Compared with the EPS, the geometric factor of the M10 instrument was large ( $14$  cm<sup>2</sup>-sr  
281 versus  $10^{-3}$  cm<sup>2</sup>-sr). Because of its large geometric factor, the M10 particle instrument was more  
282 susceptible to saturation from high-count-rate events at or below the energy threshold of the  
283 instrument. Armstrong et al. (1975, 1979) pointed out ambiguities in the data set that suggesting  
284 that the M10 particle instrument was responding to pulse pile-up from low-energy ( $>35$  keV)  
285 electrons during M10-I. In contrast, EPS is not susceptible to pile up from high-count-rate

286 events (Andrews et al., 2007), and in any case, not even low-rate events above background (~5  
287 particles/cm<sup>2</sup>/s/sr/keV at 45 keV) events were seen during any of the three MESSENGER flybys.

288 During M1, M2, and M3, solar particle activity in the inner heliosphere was very low because  
289 of the extended period of minimal solar activity. During much of the cruise period from June  
290 2007 up to M3, there were no SEP events detected by EPS except for the one on 31 December  
291 2007 (Fig. 1). It is possible that the number of low-energy suprathermal particles available in the  
292 inner heliosphere (Mason, 2000) that could interact with Mercury's magnetosphere and later be  
293 accelerated in situ (Baker 1986) was also very low. This situation could limit the intensity of  
294 high-energy particle population in Mercury's magnetosphere (e.g., Baker, 1986), and with EPS  
295 small geometric factor, we could not measure at that level. Not only has the extended period of  
296 low solar activity limited SEP seed particles for acceleration, but the IMF field has also been  
297 extremely weak. From the magnetic field measured by MAG during M2, Slavin et al. (2009b)  
298 calculated a cross-magnetosphere electric potential of about 30 kV. Although not all types of  
299 magnetospheric charged-particle acceleration processes are limited by magnetospheric potential  
300 drop, this low cross-magnetosphere potential is consistent with the lack of particles having  
301 energies larger than 35 keV as observed in the EPS data.

302 Slavin et al. (2009b) deduced that Mercury's magnetosphere is highly responsive to IMF  
303 orientation due to its small inertia. During the steady southward IMF at the time of M2,  
304 magnetic reconnection signatures (FTEs, plasmoids) were observed throughout the Mercury's  
305 magnetosphere. However, no dipolarization was observed by the MESSENGER magnetometer  
306 during M2 (or M1 or, M3). In Earth's magnetosphere, dipolarization is closely related to particle  
307 acceleration during substorm activity (Baker et al., 1996). We also note that the M10 data  
308 showed a strong field dipolarization in close conjunction with the energetic-electron events

309 (Christon, 1987; Slavin et al., 1997). The lack of high-energy particles at Mercury during  
310 reconnection may be important in understanding particle acceleration processes at Earth. During  
311 M3, several substorm-like signatures were evident in the MAG data (Slavin et al., 2010).  
312 Although a spacecraft safe-hold event stopped measurements on the outbound portion of the  
313 trajectory, no energetic electrons with energies  $> 35$  keV were detected above instrument  
314 background level during the entire inbound portion of the trajectory up to a few minutes before  
315 closest approach.

316

## 317 **5. Conclusions**

318 MESSANGER's three passages through Mercury's magnetosphere provided the first  
319 measurements of magnetospheric characteristics since the Mariner 10 flybys in 1974-1975.  
320 Mercury's small magnetosphere is highly responsive to changes in IMF orientation and solar-  
321 wind conditions. During M1, the IMF was steadily northward, no reconnection signatures were  
322 observed from the Magnetometer during the flyby, and no energetic particles higher in energy  
323 than 35 keV were detected by the EPS. Because of the southward IMF, in contrast, multiple  
324 FTEs and plasmoid signatures were observed during M2. Surprisingly, EPS again made no  
325 direct detection of energetic particles having energies above 35 keV. From this null result we are  
326 able to place an upper limit on the electron intensity at 45 keV of  $\sim 5$  particles/cm<sup>2</sup>/s/sr/keV.  
327 During M3, the IMF was highly variable prior to spacecraft entry into Mercury's magnetosphere.  
328 The MAG documented multiple tail-loading events similar to substorm-like signatures at Earth.  
329 However, a key signature of energetic-particle acceleration during substorm events at Earth, i.e.,  
330 field depolarization, was absent at Mercury.

331 The XRS instrument on MESSENGER detected X-rays produced by low-energy electrons  
332 during both M1 and M2. We used a kappa distribution for the electrons to model the XRS  
333 instrument response and found good agreement between modeled absolute electron intensity and  
334 the upper limit given by EPS measurement except for one event during M2, for which the XRS-  
335 derived flux is 100 times higher than the EPS upper limit (Fig. 6). However, we found that the  
336 local magnetic field orientation during that XRS spike made detection of this short-duration  
337 electron event difficult to see with EPS, implying that the electron pitch-angle distribution was  
338 narrowly peaked near 90°.

339  
340 **Acknowledgments.** The authors acknowledge the large number of scientists and engineers at  
341 The Johns Hopkins University Applied Physics Laboratory who contributed their technical  
342 expertise and skill to the successful development of the EPS sensor. Resources supporting the  
343 XRS analysis were provided by the NASA High-End Computing (HEC) Program through the  
344 NASA Center for Computational Sciences (NCCS) at the Goddard Space Flight Center. The  
345 MESSENGER project is supported by the NASA Discovery Program under contracts NASW-  
346 00002 to the Carnegie Institution of Washington and NAS5-97271 to the Johns Hopkins  
347 University Applied Physics Laboratory.

348

349 **References**

- 350 Adler, I. and Trombka, J.I., 1977. Orbital chemistry – Lunar surface analysis from the X-  
351 ray and gamma ray remote sensing experiments. *Phys. Chem. Earth* 10, 17–43.  
352
- 353 Anderson, B.J., Acuña, M.H., Korth, H., Purucker, M.E., Johnson, C.L., Slavin, J.A.,  
354 Solomon, S.C., McNutt, R.L., Jr., 2008. The structure of Mercury’s magnetic field  
355 from MESSENGER’s first flyby. *Science* 321, 84–88.  
356
- 357 Andrews, G.B., Zurbuchen, T.H., Mauk, B.H., Malcom, H., Fisk, L.A., Gloeckler, G. Ho,  
358 G.C., Kelley, J.S., Koehn, P.L., LeFevere, T.W., Livi, S. S., Lundgren, R.A., Raines,  
359 J.M., 2007. The Energetic Particle and Plasma Spectrometer instrument on the  
360 MESSENGER spacecraft. *Space Sci. Rev.* 131, 523–556.  
361
- 362 Armstrong, T.P., Krimigis, S.M., Lanzerotti, L.J., 1975. A reinterpretation of the reported  
363 energetic particle fluxes in the vicinity of Mercury. *J. Geophys. Res.* 80, 4015–4017.  
364
- 365 Armstrong, T.P., Krimigis, S.M., Lanzerotti, L.J., 1979. Comment on ‘Electron calibration of  
366 instrumentation for low-energy high-intensity particle measurements at Mercury’ by Christon,  
367 Daly, Eraker, Perkins, Simpson, and Tuzzolino. *J. Geophys. Res.* 84, 4468–4470.  
368
- 369 Baker, D.N., 1986. Jovian electron populations in the magnetosphere of Mercury. *Geophys. Res.*  
370 *Lett.* 13, 789-792.  
371
- 372 Baker, D.N., T.I. Pulkkinen, T.I., Angelopoulos, V., Baumjohann, W., McPherron, R.L., 1996.  
373 Neutral line model of substorms: Past results and present view. *J. Geophys. Res.* 101, 12,975–  
374 13,010.  
375
- 376 Baker, D.N., Odstrcil, D., Anderson, B.J., Arge, C.N., Benna, M., Gloeckler, G., Raines, J.M.,  
377 Schriver, D., Slavin, J.A., Solomon, S.C., Killen, R.M., Zurbuchen, T.H., 2009. Space  
378 environment of Mercury at the time of the first MESSENGER flyby: Solar wind and  
379 interplanetary magnetic field modeling of upstream conditions. *J. Geophys. Res.* 114,  
380 A10101, doi:10.1029/2009JA014287.  
381
- 382 Baker, D.N., Odstrcil, D., Anderson, B.J., Arge, C.N., Benna, M., Gloeckler, G., Raines, J.M.,  
383 Mayer, L.R., Raines, J.M., Schriver, D., Slavin, J.A., Solomon, S.C., Zurbuchen, T.H., 2010.  
384 The space environment of Mercury at the times of the second and third MESSENGER flybys.  
385 *Planet. Space Sci.*, this issue.  
386
- 387 Christon, S.P., 1987. A comparison of the Mercury and Earth magnetospheres: Electron  
388 measurements and substorm time scales. *Icarus* 71, 448–471.  
389
- 390 Eraker, J.H., Simpson, J.A., 1979. Jovian electron propagation close to the Sun (~0.5 AU).  
391 *Astrophys. J.* 232, L131–L134.  
392

393 Feldman, W., Lawrence, D.J., Goldsten, J.O., Gold, R.E., Baker, D.N., Haggerty, D.K.,  
394 Ho, G.C., Krucker, S., Lin, R.P., Mewaldt, R.A., Murphy, R.J., Nittler, L.R., Rhodes,  
395 E.A., Slavin, J.A., Solomon, S.C., Starr, R. D., Vilas, F., Vourlidas, A., 2010.  
396 Evidence for extended acceleration of solar flare ions from 1–8 MeV solar neutrons  
397 detected with the MESSENGER Neutron Spectrometer. *J. Geophys. Res.* 115,  
398 A01102, doi:10.1029/2009JA014535.  
399

400 Luhmann, J.G., Russell, C.T., Tsyganenko, N.A., 1998. Disturbances in Mercury’s  
401 magnetosphere: Are the Mariner 10 “substorms” simply driven?, *J. Geophys. Res.* 103, 9113–  
402 9120.  
403

404 Mason, G.M., 2000. Composition and energy spectra of ions accelerated in corotating interaction  
405 regions. In: Mewaldt, R.A., Jokipii, J.R., Lee, M.A., Möbius, E., Zurbuchen, T.H. (Eds),  
406 Acceleration and transport of energetic particles observed in the heliosphere: ACE 2000  
407 Symposium. AIP Conference Proceedings, vol. 528, American Institute of Physics, Melville,  
408 N.Y., pp. 234–241.  
409

410 Mukai, T., Ogasawara, K., Saito, Y., 2004. An empirical model of the plasma environment  
411 around Mercury. *Adv. Space Res.* 33, 2166–2171.  
412

413 Ness, N.F., Behannon, K.W., Lepping, R.P., Whang, Y.C., Schatten, K.H., 1974, Magnetic field  
414 observations near Mercury: Preliminary results from Mariner 10, *Science* 185, 151–160.  
415

416 Pelowitz, D.B. (Ed.), 2005. Monte Carlo N-Particle eXtended (MCNPX) User’s Manual  
417 Version 2.5.0. Report LA-UR-94-1817, Los Alamos National Laboratory, Los  
418 Alamos, N. Mex.  
419

420 Russell, C.T., Baker, D.N., Slavin, J.A., 1988. The magnetosphere of Mercury. In: Vilas, F.,  
421 Chapman, C.R., Matthews, M.S. (Eds.), *Mercury*. University of Arizona Press, Tucson, pp.  
422 514–561.  
423

424 Schlemm, C.E., II, Starr, R.D., Ho, G.C., Bechtold, K.E., Hamilton, S.A., Boldt, J.D.,  
425 Boynton, W.V., Bradley, W., Fraeman, M.E., Gold, R.E., Goldsten, J.O., Hayes, J.R.,  
426 Jaskulek, S.E., Rossano, E., Rumpf, R.A., Schaefer, E.D., Strohbahn, K., Shelton,  
427 R.G., Thompson, R.E., Trombka, J.I., Williams, B.D., 2007. The X-Ray Spectrometer  
428 on the MESSENGER spacecraft. *Space Sci. Rev.* 131, 393–415.  
429

430 Simpson, J.A., Eraker, J.H., Lamport, J.E., Walpole, P.H., 1974. Electrons and protons  
431 accelerated in Mercury’s magnetic field. *Science* 185, 160–166.  
432

433 Slavin, J.A., Owen, J.C.J., Connerney, J.E.P., Christon, S.P., 1997. Mariner 10  
434 observations of field-aligned currents at Mercury. *Planet. Space Sci.* 45, 133–141.  
435

436 Slavin, J., Acuña, M.H., Anderson, B.J., Baker, D.N., Benna, M., Gloeckler, G., Gold,  
437 R.E., Ho, G.C., Killen, R.M., Korth, H., Krimigis, S.M., McNutt Jr., R.L., Nittler,  
438 L.R., Raines, J.M., Schriver, D., Solomon, S.C., Starr, R.D., Trávníček, P., Zurbuchen,

439 T.H., 2008. Mercury's magnetosphere after MESSENGER's first flyby. *Science* 321,  
440 85–89.  
441

442 Slavin, J.A., Anderson, B.J., Zurbuchen, T.H., Baker, D.N., Krimigis, S.M., Acuña,  
443 M.H., Benna, M., Boardsen, S.A., Gloeckler, G., Gold, R.E., Ho, G.C., Korth, H.,  
444 McNutt, R.L., Jr., Raines, J.M., Sarantos, M., Schriver, D., Solomon, S.C., Trávníček,  
445 P., 2009a. MESSENGER observations of Mercury's magnetosphere during northward  
446 IMF. *Geophys. Res. Lett.* 36, L02101, doi:10.1029/2008GL036158.  
447

448 Slavin, J.A., Acuña, M.H., Anderson, B.J., Baker, D.N., Benna, M., Boardsen, S.A.,  
449 Gloeckler, G., Gold, R.E., Ho, G.C., Korth, H., Krimigis, S.M., McNutt, R.L., Jr.,  
450 Raines, J.M., Sarantos, M., Schriver, D., Solomon, S.C., Trávníček, P., Zurbuchen,  
451 T.H., 2009b. MESSENGER observations of magnetic reconnection in Mercury's  
452 magnetosphere. *Science* 324, 606–610.  
453

454 Slavin, J.A., Anderson, B.J., Baker, D.N., Benna, M., Boardsen, S.A., Gloeckler, G.,  
455 Gold, R.E., Ho, G.C., Korth, H., Krimigis, S.M., McNutt, R.L., Jr., Nittler, L.R.,  
456 Raines, J.M., Sarantos, M., Schriver, D., Solomon, S.C., Starr, R.D., Trávníček, P.,  
457 Zurbuchen, T.H., 2010. MESSENGER observations of extreme loading and unloading  
458 of Mercury's magnetic tail. *Science*, 329, 665–668.  
459

460 Solomon, S.C., McNutt, R.L., Jr., Gold, R.E., Domingue, D.L., 2007. MESSENGER  
461 mission overview. *Space Sci. Rev.* 131, 3–39.  
462

463 Starr, R., Clark, P.E., Murphy, M.E., Floyd, S.R., McClanahan, T.P., Nittler, L.R.,  
464 Trombka, J.I., Evans, L.G., Boynton, W.V., Bailey, S.H., Bhangoo, J., Mikheeva, I.,  
465 Brückner, J., Squyres, S.W., McCartney, E.M., Goldsten, J.O., McNutt, R.L., 2000.  
466 Instrument calibrations and data analysis procedures for the NEAR X-ray  
467 spectrometer. *Icarus*, 147, 498–519.  
468

469 Wurz, P., Blomberg, L., 2001. Particle populations in Mercury's magnetosphere. *Planet*  
470 *Space Sci.* 49, 1643–1653.  
471  
472  
473  
474  
475  
476  
477

478

479 **Fig. 1.** A C8-class solar flare was detected by EPS on 31 December 2007, two weeks before the  
480 first MESSENGER flyby of Mercury. Energetic electrons from the flare are shown for three  
481 energy intervals..

482

483 **Fig. 2.** Overview of the energetic particle, magnetic field, and X-ray measurements during M1.  
484 During the passage of the spacecraft through Mercury's magnetosphere, the IMF was generally  
485 northward. EPS has six look directions along the spacecraft Z-Y plane. Sectors 2 and 3 are the  
486 two look directions that are above and below the spacecraft X-Y plane, respectively, each  
487 covering  $22^\circ$  of the FOV. No energetic particles were detected by EPS at any time during the  
488 flyby. The XRS data, plotted in the bottom panel, show the single fluorescence event (M1-E1)  
489 detected. The three components of the in-situ magnetic field are plotted in Mercury solar orbital  
490 (MSO) coordinates:  $X_{MSO}$  points from the center of the planet to the Sun;  $Y_{MSO}$  is positive in the  
491 direction opposite to orbital motion; and  $Z_{MSO}$  is positive to the north and perpendicular to the  
492 Mercury's orbital plane. Magnetospheric boundaries crossed include the inbound and outbound  
493 bow shock (BS) and magnetopause (MP); closest approach is denoted by CA. Radial distance  
494 from Mercury is measured in units of Mercury's radius ( $R_M$ ).

495

496 **Fig. 3.** Energy spectra determined by EPS before, during, and after the closest approaches for (a)  
497 M1, (b) M2, and (c) M3. The legends denote the time and radial distance when the 300-s-  
498 averaged spectra were taken during each flyby. There was a small change in the energy channels  
499 on EPS between the first two flybys, the result of new flight software uploaded to EPS in August  
500 2008. Note, however, that the shape of the energy spectrum is essentially the same during each  
501 flyby. The energy peak near 150 keV for all flybys is the result of high-energy cosmic rays  
502 penetrating the solid-state detectors from all directions.

503

504 **Fig 4.** Overview of the energetic particle, magnetic field, and X-ray measurements during M2.  
505 Despite the steady southward IMF and the documentation of multiple reconnection events by the  
506 Magnetometer, no major energetic particle events were detected by EPS. The drop in particle  
507 intensity at closest approach corresponds to the shadowing effect of the planet on the cosmic-ray  
508 background. The XRS data show two electron-induced fluorescence events during the flyby  
509 (M2-E1 and M2-E2). For other labels see Fig. 2.

510

511 **Fig. 5.** Overview of the energetic particle, magnetic field, and X-ray measurements during M3.  
512 A spacecraft safe-hold event occurred a few minutes before closest approach, and no science  
513 data were collected after this event. The XRS data show a small electron-induced fluorescence  
514 event shortly before data flow was halted.

515

516 **Fig. 6.** Comparison of modeled (blue) and measured (red) XRS spectra for event M1-E1 (left  
517 column) and for event M2-E2 (right column). The incidence angles with respect to GPC normal  
518 for M1-E1 and M2-E2 are  $0^\circ$  and  $6^\circ$ , respectively. Parameters used to produce the modeled  
519 results are given in Table 1.

520

521 **Fig. 7.** Electron flux inferred from XRS measurements. The flux for M2-E1 (red curve) and for  
522 M1-E1 (not shown) are consistent with the EPS lower limit. The flux for M2-E2 at 45 keV is  
523  $\sim 100$  times greater than the EPS limit, indicated by the asterisk.

524  
525  
526  
527  
528  
529  
530  
531  
532  
533  
534

**Fig. 8.** : (a) Sketch of the EPS and XRS FOVs in the spacecraft coordinate system. The XRS FOV is conical ( $12^\circ$  full angle) along the spacecraft +Z direction, whereas the EPS has a fan-shaped FOV that looks away from the spacecraft sunshade along the +Y direction. The two FOVs do not overlap. Also shown is the orientation of the local magnetic field as measured by MESSENGER during event M2-E2. (b) XRS count rates on the three gas proportional counters during M2 and the angle (red) between the local magnetic field and the spacecraft Z-axis (or XRS collimator axis). The two electron-induced fluorescence events during M2 (M2-E1 and M2-E2) are indicated by vertical dashed lines.

**Table 1.** Parameters used to fit the XRS electron events detected during M1, M2 and M3.

Event	Date	Time of event (UTC)	Duration (s)	$N$  (electrons/cm <sup>2</sup> -sr-s-keV)	Best-fit $K$	Best-fit $E_o$
M1-E1	14 January 2008	18:59:49	180	$1.35 \times 10^7$	8	0.7
M2-E1	6 October 2008	08:35:08	60	$5.39 \times 10^7$	8	0.7
M2-E2	6 October 2008	08:47:08	120	$3.06 \times 10^8$	7	1.0
M3-E1	29 September 2009	21:45:39	60	$3.85 \times 10^6$	8	0.7

Note: A kappa distribution (Christon, 1987) is assumed, where the electron flux is given by

$j_e = N[E/E_o][1 + E/KE_o]^{K-1}$ , and where  $N$ ,  $E_o$  and  $K$  are the normalization factor, modal energy, and kappa, respectively.



Figure 1:

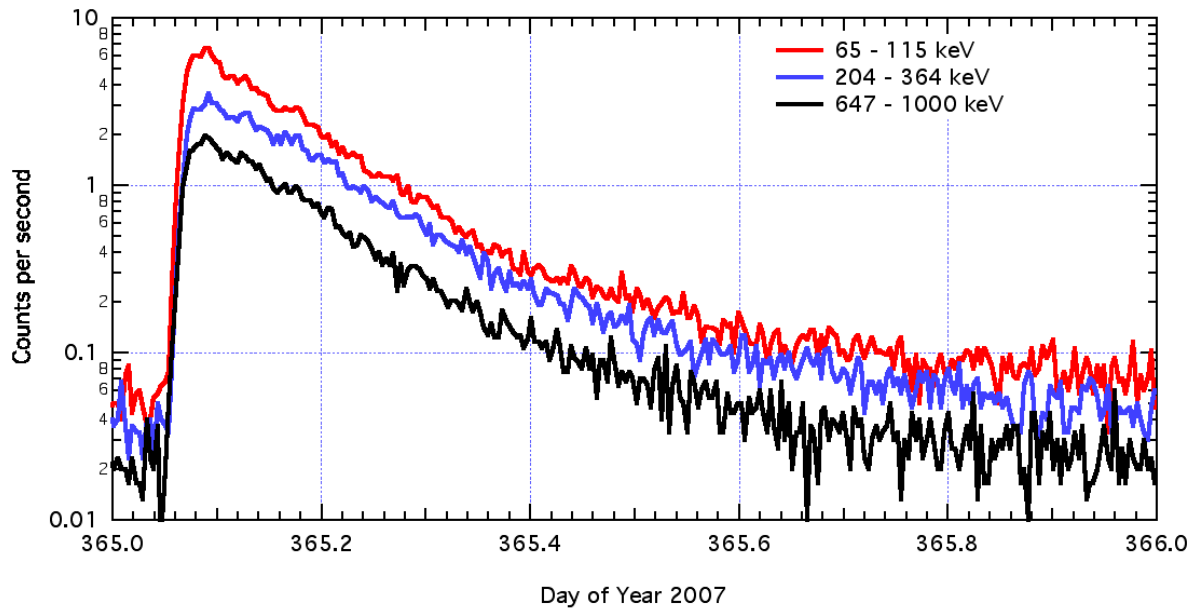


Figure 1

Figure 2:

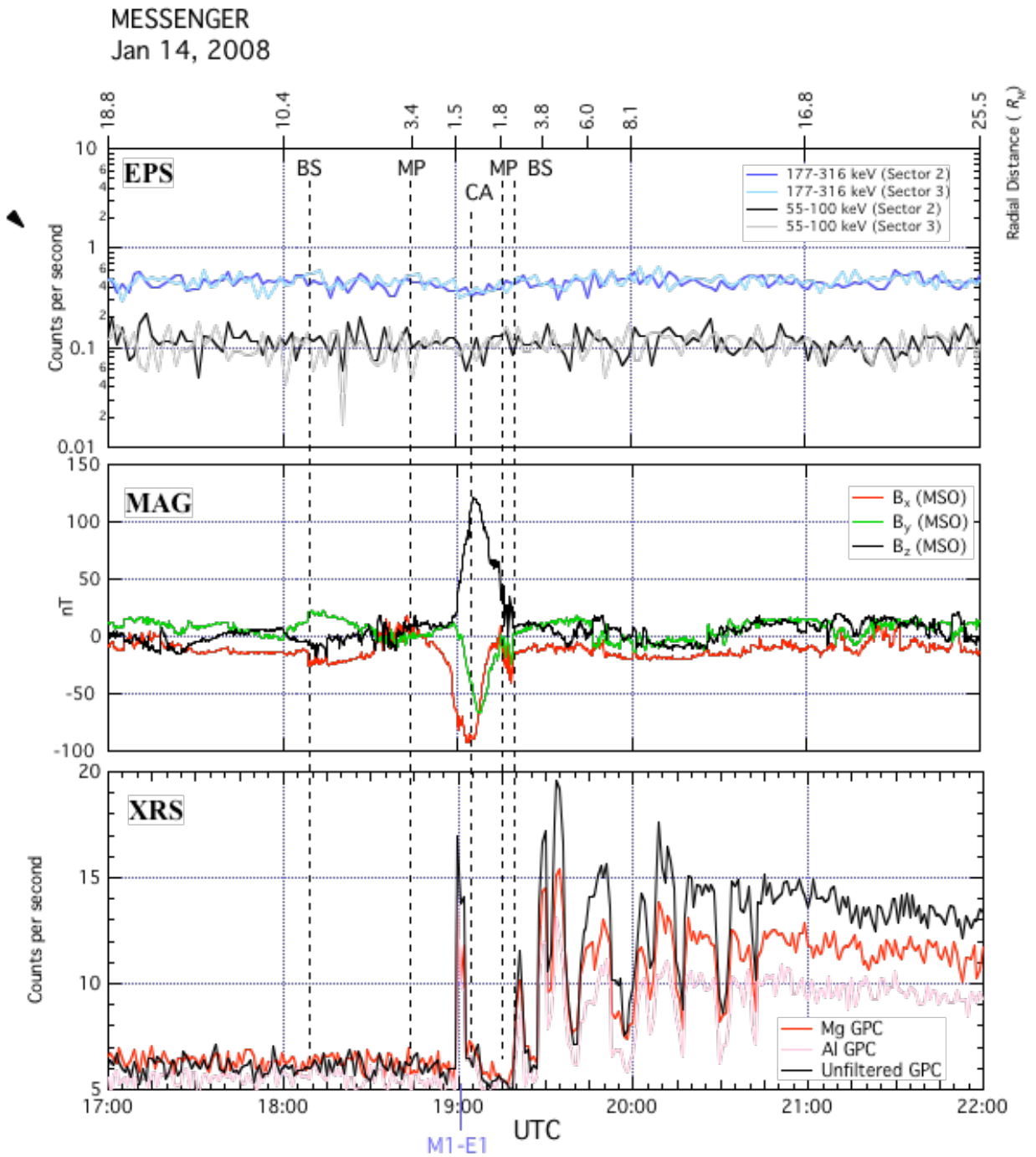


Figure 2

Figure 3:

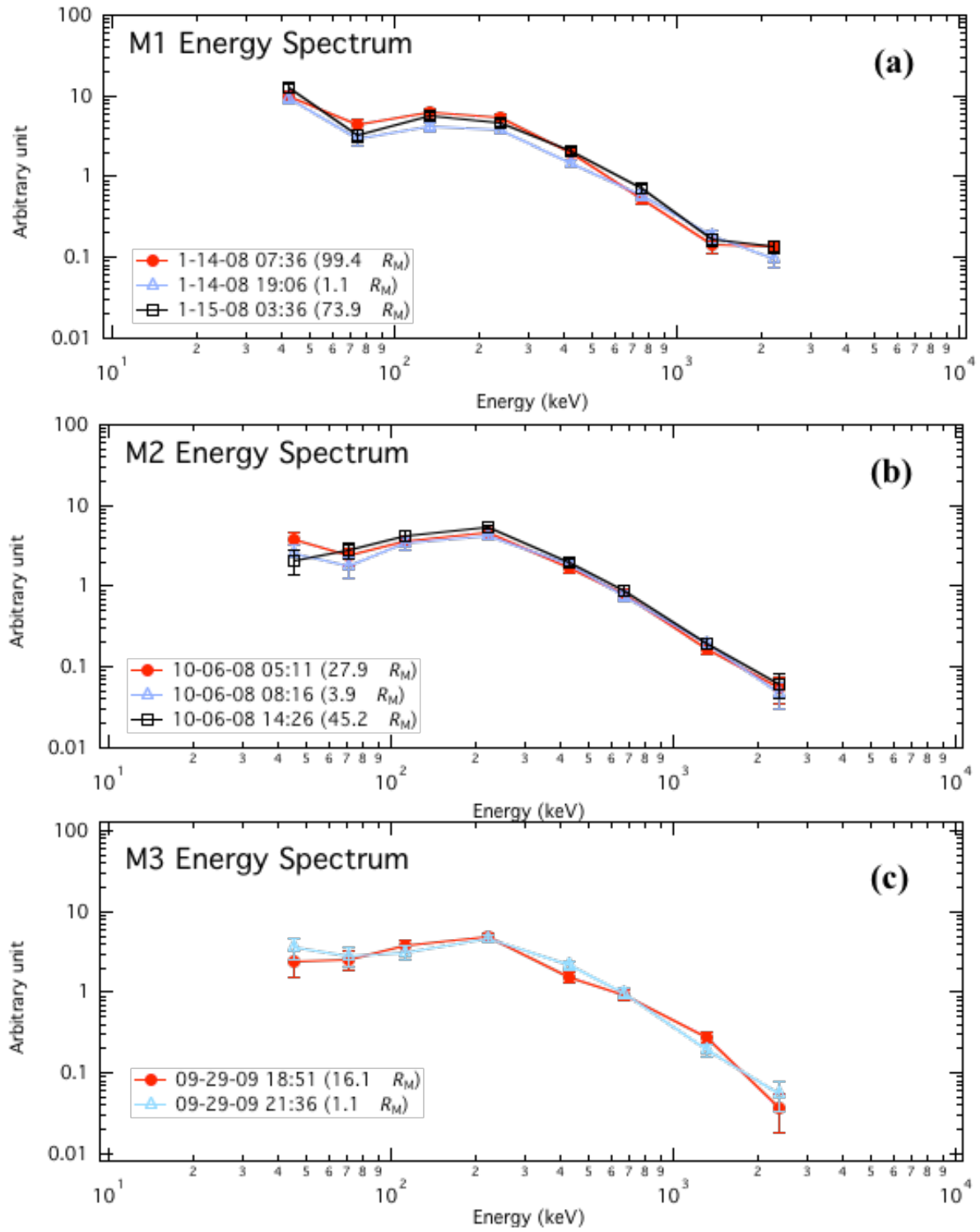


Figure 4:

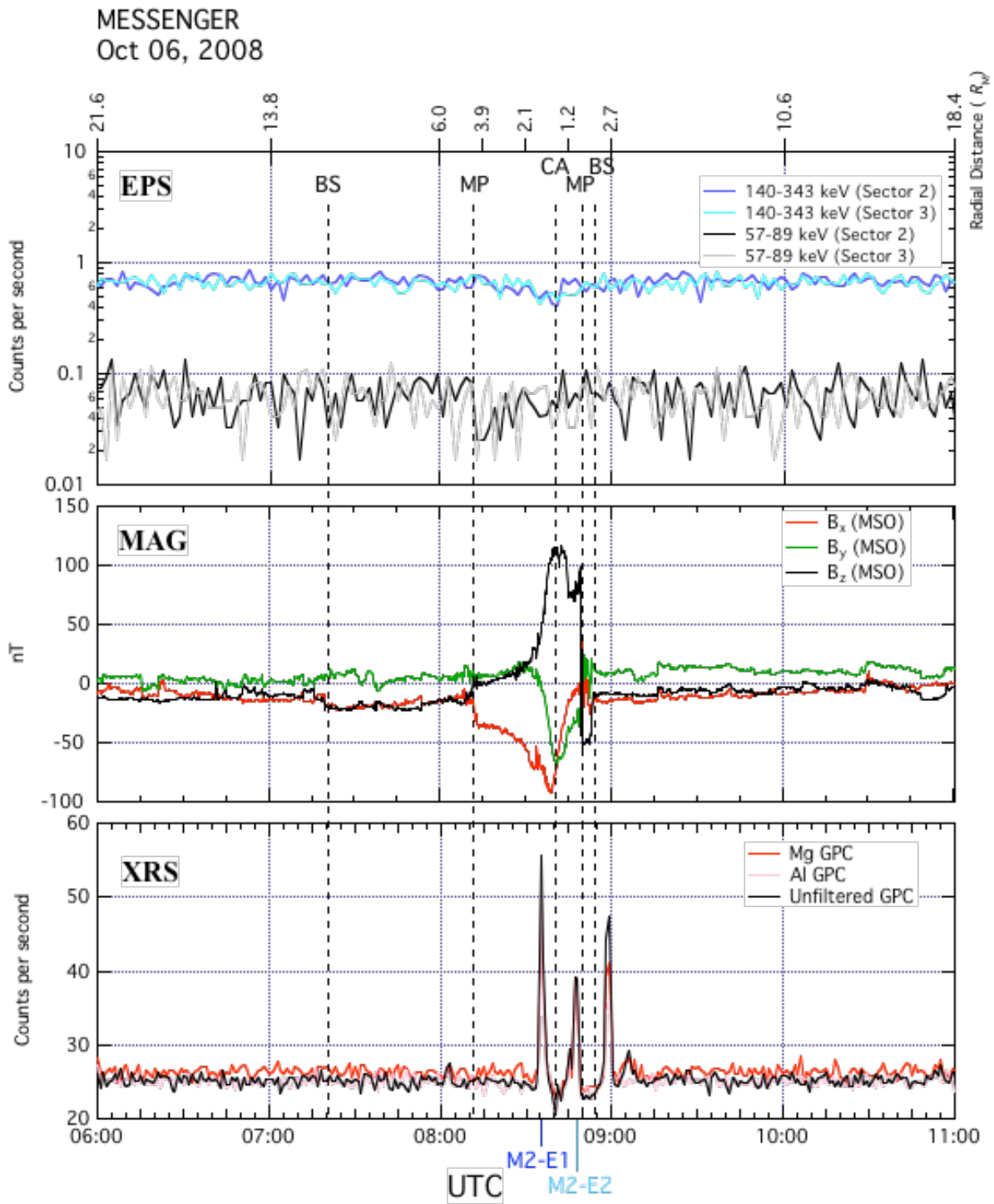


Figure 4

Figure 5.

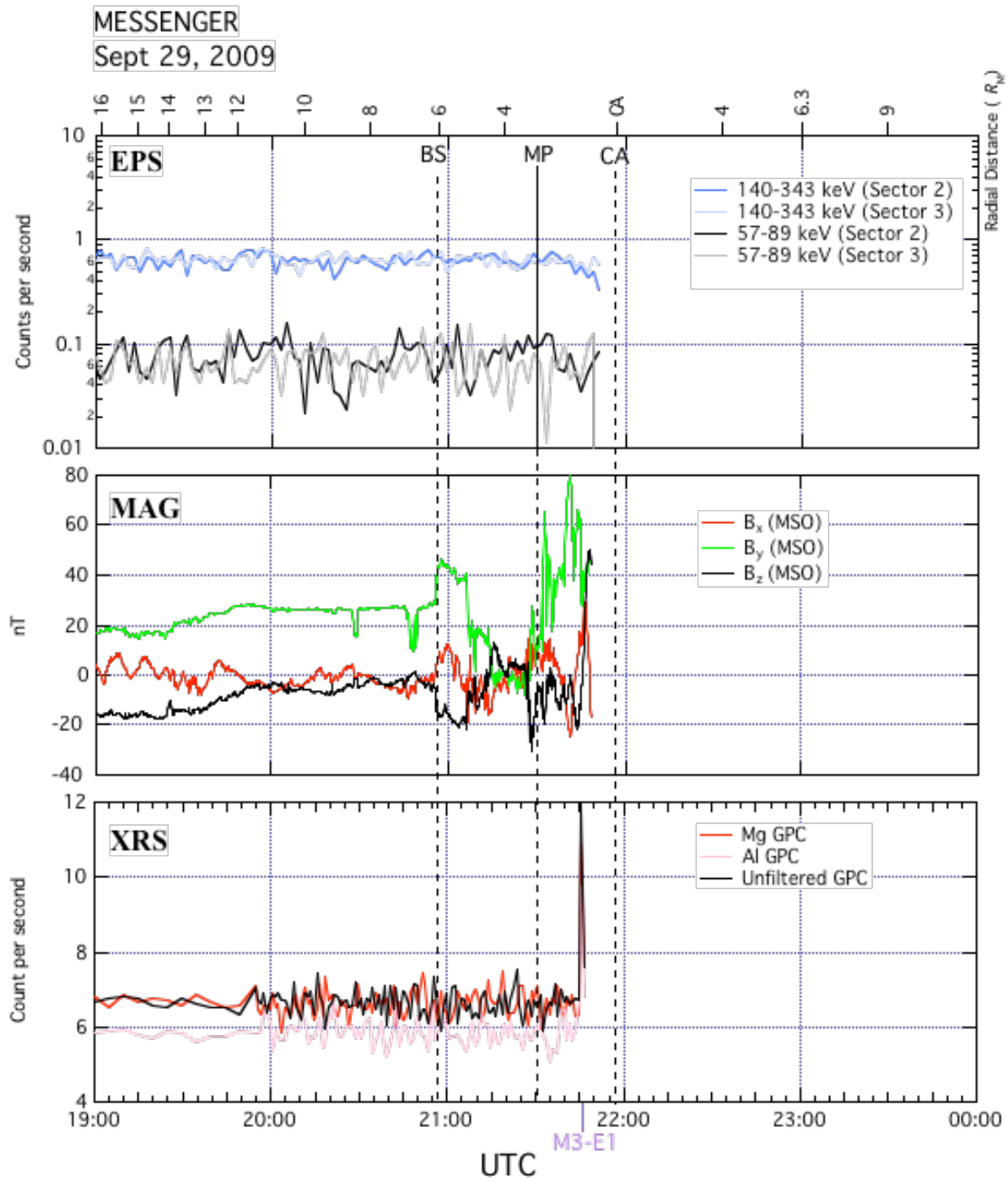


Figure 5

Figure 6

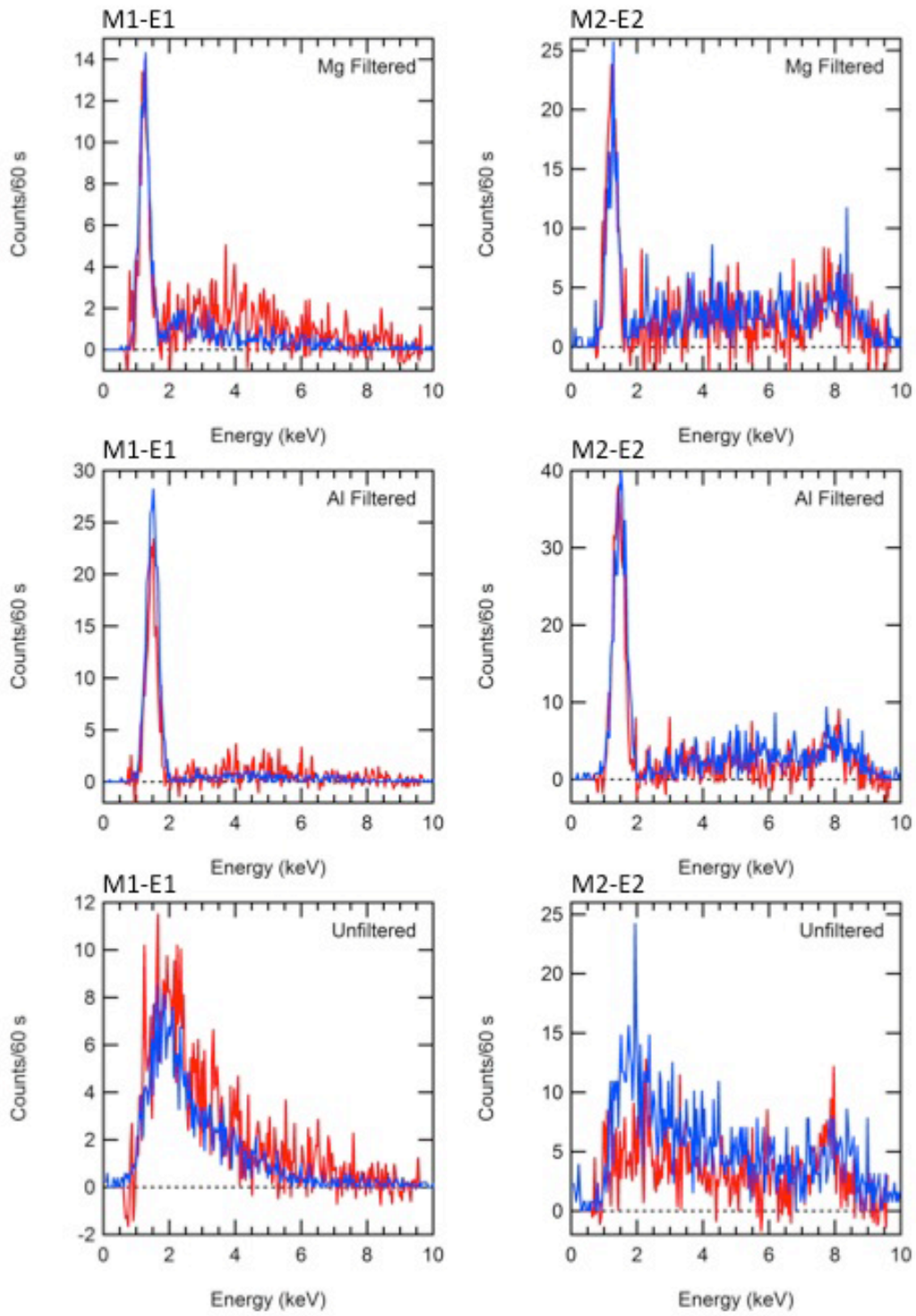


Figure 7.

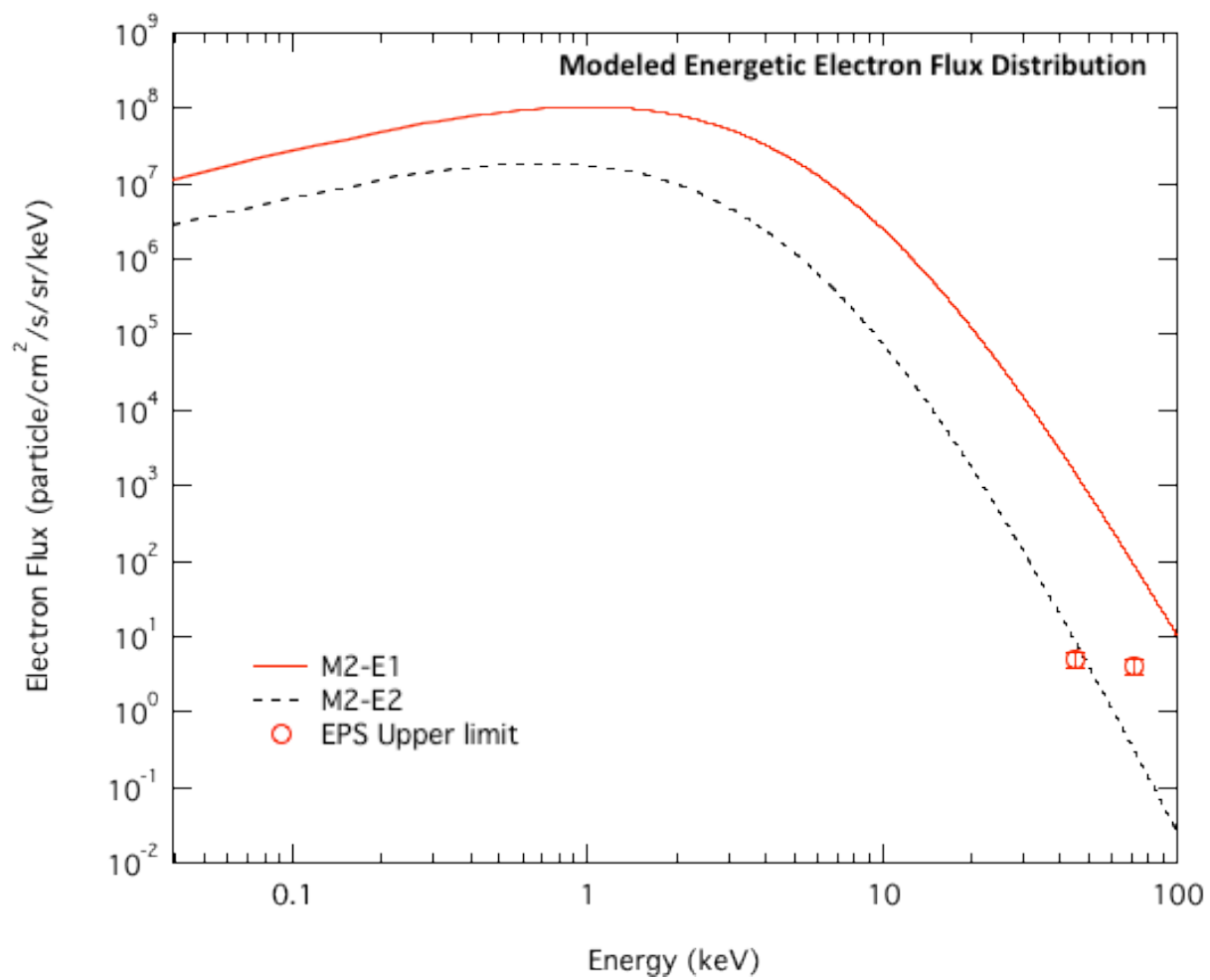


Figure 8:

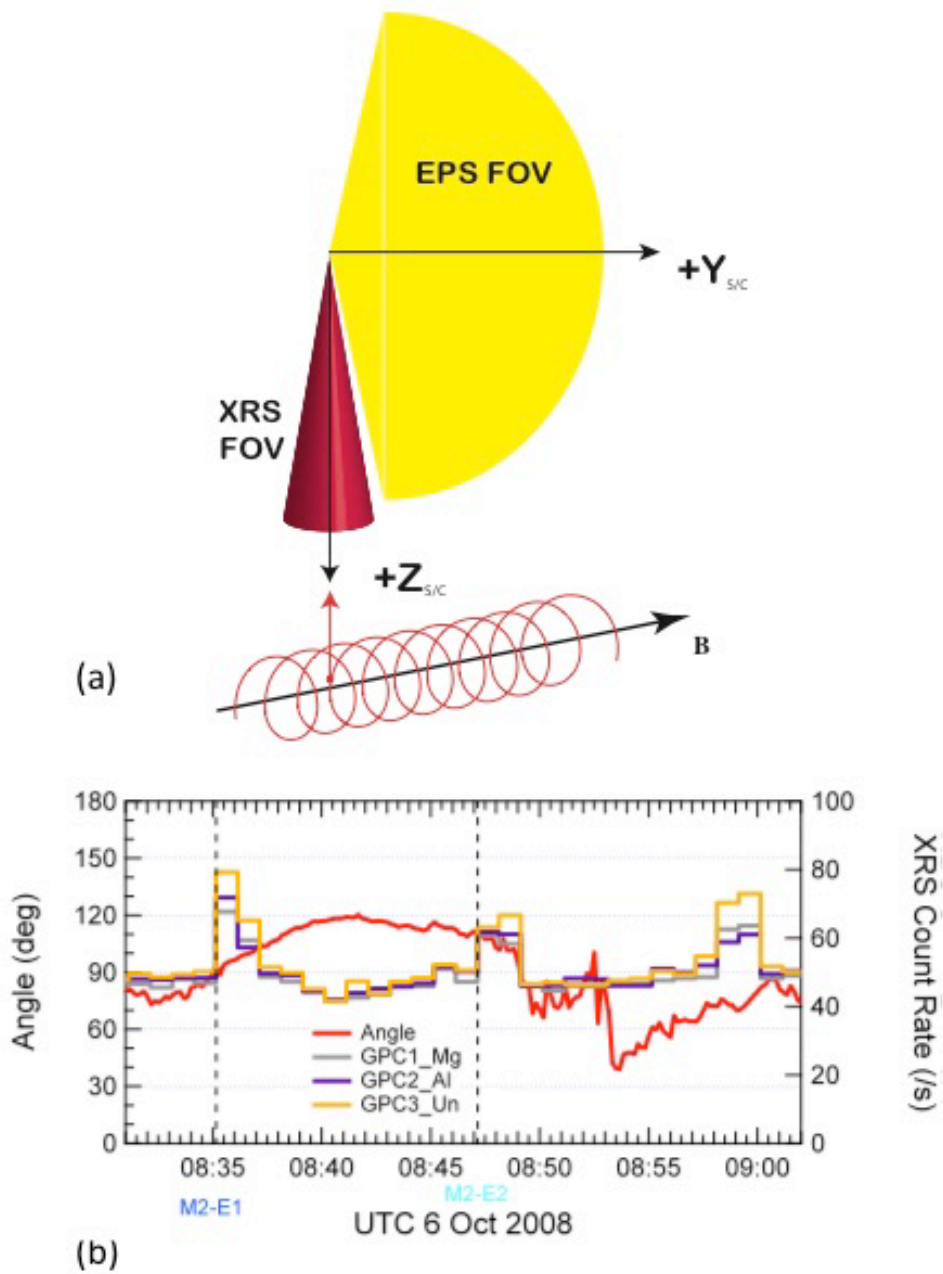


Figure 8